Journal of Non-Crystalline Solids 357 (2011) 1328–1334

Contents lists available at ScienceDirect

Journal of Non-Crystalline Solids

journal homepage: www.elsevier.com/ locate/ jnoncrysol

Thermal, chemical, optical properties and structure of Er^{3+}-doped and Er^{3+}/Yb^{3+}-codoped P_2O_5–Al_2O_3–ZnO glasses

S.W. Yung [a,*], S.M. Hsu [b], C.C. Chang [a], K.L. Hsu [a], T.S. Chin [c], H.I. Hsiang [d], Y.S. Lai [a]

[a] Department of Materials Science and Engineering, National United University, Miao-Li, 36003, Taiwan
[b] Department of Biomedical Imaging and Radiological Science, China Medical University, Taichung, Taiwan
[c] Department of Materials Science and Engineering, Feng Chia University, Taichung, Taiwan
[d] Department of Materials Science and Engineering, National Cheng Kung University, Tainan, Taiwan

ARTICLE INFO

Article history:
Received 29 June 2010
Received in revised form 26 November 2010
Available online 13 January 2011

Keywords:
Phosphate glass;
Er^{3+}/Yb^{3+}-codoping;
Fluorescence;
Absorption cross-section;
Emission cross-section

ABSTRACT

This study was explored in series of the optical, thermal, and structure properties based on $60P_2O_5$–$10Al_2O_3$–30ZnO (PAZ) glasses system that doped with varied rare-earth (RE) elements Yb_2O_3/Er_2O_3. The glass transition temperature, softening temperature and chemical durability were increased with RE-doping concentrations increasing, whereas thermal expansion coefficient was decreased. In the optical properties, the absorption and emission intensities also increase with RE-doping concentrations increasing, When Er_2O_3 and Yb_2O_3 concentrations are over than 3 mol% in the Er^{3+}-doped PAZ system and Yb^{3+}-doped concentration is over than 3 mol% for Er^{3+}/Yb^{3+}-codoped PAZ system, the emission intensity significantly decreases presumably due to concentration quenching, formation of the ions clustering, and OH^- groups in the glasses network. It is suggested that the maximum emission cross-section (σ_e) is 7.64×10^{-21} cm^2 at 1535 nm is observed for 3 mol% Er^{3+}-doped PAZ glasses. Moreover, the maximum $\sigma_e\times$full-width-at-half-maximum is 327.8 for 5 mol% Er^{3+}-doped PAZ glasses.

1. Introduction

Phosphate glasses have lower glass transition temperature (T_g), lower melting temperature (T_m), higher thermal expansion coefficients (α)[1–3], lower optical dispersions, and good UV transparency than most silicate glasses[4,5]. These properties make them suitable for many applications, such as waveguide amplifier [5], specialty sealing [6], nuclear waste glasses [7,8] and laser applications [5,9]. However, these glasses have a relatively poor chemical durability that often limits their usefulness [10,11]. According to previous studies, the chemical durability of phosphate glasses can be improved by the addition of various rare-earth ions such as Er^{3+} and Yb^{3+} ions [12,13].

Rare-earth doped phosphate glasses have been extensively investigated in recent years. In particular, erbium-doped phosphate glasses are interesting materials for amplifiers, wavelength division multiplexing and optical communication systems at 1.5 μm [14–16]. The energy levels of the Er^{3+} ions for optical amplification at 1.5 μm form a three-level system which requires a high pump rate to achieve population inversion. On the other hand, the concentration of Er^{3+} in the glass must be as higher as possible [17]. However, the higher non-radiative losses incur when Er^{3+} concentration is beyond a critical value. In addition, the pumping efficiency and absorption cross-section of Er^{3+} in glasses are rather low. Therefore, codoping with sensitizer ions is usually required [18]. Yb^{3+} is a well-known sensitizer to enhance the absorption and pumping efficiency of Er^{3+} doped phosphate glasses, due to the fact that $^2F_{7/2}\rightarrow{}^2F_{5/2}$ transition in spectral region of the Yb^{3+} overlaps the $^4F_{15/2}\rightarrow{}^4F_{11/2}$ transition of the Er^{3+}. Such an effective transfer of the excitation energy prevails from ytterbium to erbium [19,20]. At the same time, Yb^{3+} ions exhibit high stimulated emission cross-section and a broad absorption band between 800 and 1100 nm [21].

Zhang et al. studied spectroscopic properties and energy transfer in Er^{3+}/Yb^{3+}-doped phosphate glasses [22]. They indicated that the intensity of fluorescence emission of Er^{3+}/Yb^{3+}-codoped phosphate glass is much higher than that of Er^3 single-doped phosphate glass. Chen et al. indicated that the Yb^{3+} ions can absorb more efficiently the 980 nm light and transfer the energy to Er^{3+} in heavily Er-doped silica optical fibers [23]. The phenomenon increases the population of $^4I_{11/2}$ level and induces promotion of photo-luminescence efficiency at 1540 nm. However, in accordance with the literatures [12,23,24], excess rare-earth ions in many crystals, fiber amplifiers and glass systems causes the reduction of optical properties. This arises from two reasons, the concentration quenching and the formation of ions clustering. Therefore, the glass with optimum dopant concentration of rare-earth ions is very important. At present, several researches explored the effect of Er^{3+} on optical properties and energy transfer. Up to now there are only a few researches of the effects of Er^{3+} and Yb^{3+} concentrations on optical properties and structure. The purposes

* Corresponding author. Tel.: +886 37 382521.
E-mail address: hwyang@nuu.edu.tw (S.W. Yung).

0022-3093/$ – see front matter © 2010 Elsevier B.V. All rights reserved.
doi:10.1016/j.jnoncrysol.2010.12.011

of this study mainly focused on examining effects of Er^{3+} and Er^{3+}/Yb^{3+} concentrations on structure and properties of P_2O_5–Al_2O_3–ZnO glasses. Yb^{3+} was used as a sensitizer for Er^{3+} to improve the pumping absorption and the quantum efficiency. Structure evidenced from emission spectra and absorption spectra; density, thermal stability, coefficient of thermal expansion and chemical durability of Er^{3+}-doped and Er^{3+}/Yb^{3+}-codoped P_2O_5–Al_2O_3–ZnO host glasses were investigated.

2. Experimental

2.1. Preparation of specimens

A series of zinc aluminum phosphate glasses were prepared by raw materials $NH_4H_2PO_4$ (Mallinckrodt Baker Company), $Al(OH)_3$ (Mallinckrodt Baker Company), ZnF_2 (Aldrich Chemical Company), Er_2O_3, and Yb_2O_3 (Johnson Matthey Company) with various molar ratios. The basic composition of the studied glass is, in mole fraction, PAZ doping with Er_2O_3 and Er_2O_3/Yb_2O_3 at different concentrations. The PAZE glasses were Er_2O_3 added to replace ZnO: $60P_2O_5$–$10Al_2O_3$–(30−x) ZnO–x Er_2O_3 (x = 1, 2, 3, 4, 5, and 10 molar fractions). The PAZEY glasses were fixed at 5% Er_2O_3 with Yb_2O_3 added to replace more ZnO: $60P_2O_5$–$10Al_2O_3$–(25−y) ZnO–$5Er_2O_3$–yYb_2O_3 (y = 1, 2, 3, and 4 molar fractions). Well-mixed powders were taken into an alumina crucible, melting in an electric furnace, heated from room temperature to 1350 °C with a heating rate 10 °C/min. The melts were cast onto a pre-heated stainless steel plates and then immediately annealed for 5 h at a temperature 10 °C above T_g to release the residual thermal stress.

2.2. Density and chemical durability

Density of the PAZ, PAZE and PAZEY glasses were measured by the Archimedes method (apparent weight loss) with distilled water as the immersion fluid at 25 °C. Each specimen was cut into a cubic shape and polished with 1, 0.3, and 0.05 μm aluminum slurries. The final size of these specimens is $10\times10\times5$ mm^3. Chemical durability of the studied glasses was determined by measuring the weight loss after immersion in distilled water at 100 °C for 1 h. The ratio of specimen surface area to the immersion water amount is about 0.01 cm^2/g. The dissolution rate was defined as the weight loss per unit surface area per unit time (g/cm^2 min). Two samples were measured and the average density is reported. The relative error in these measurements was about ±0.005 g/cm^3.

2.3. Thermal properties

The glass transition temperature (T_g), glass softening temperature (T_s) and thermal expansion coefficient (α) of the studied glasses were measured by Perkin Elmer TMA 7 thermal mechanical analyzer (TMA) (Shelton, CT, USA). The TMA was calibrated using standards and expansion coefficient was calculated from 100 °C to 350 °C. The specimens were heated from room temperature with a heating rate of 10 °C/min to determine the characteristic properties. Most of the TMA measurements were made in duplicate to estimate the experimental error, and the estimated uncertainties of these characteristic temperature are ±3 °C.

2.4. Nuclear magnetic resonance (NMR) spectra

^{27}Al MAS-NMR spectrum was recorded with a Bruker DSX-400 solid state high resolution spectrometer operating at 9.4 T. The spinning rate varied between 7 and 11.5 kHz. ^{27}Al MAS-NMR spectrum was recorded at 104.1 MHz with 1 μs pluses and 1 s recycling times. Over 10,000 scans were collected for each spectrum. The ^{27}Al chemical shifts were measured versus that of an aqueous sample of 1.0-M $AlCl_3$.

2.5. Fourier transformed infrared (FTIR) spectra

The FTIR spectra of the studied glasses were measured utilizing a Bomen DA 8 spectrometer with a resolution of 4 cm^{-1}, in the frequency range 400–1400 cm^{-1} at room temperature. These specimens were ground to fine powder and mixed with dry KBr in the ratio 1:100 by weight. The mixtures were then pressed to form thin pellets under a pressure of 15 tons for a few minutes.

2.6. Absorption spectra and fluorescence spectra

The absorption spectra of the studied glasses were measured using a Shimadzu UV-3101PC spectrophotometer (Kyoto, Japan) with ±0.1 nm resolution bandwidth and ±0.3 nm wavelength accuracy, in the scanning range 850–1650 nm. Fluorescence spectra were recorded using a HORIBA Jobin Yvon TRIAX 550 spectrophotometer (Edison, NJ, USA) with a resolution of 0.025 nm, in the wavelength range 1400–1700 nm. PAZEY specimens were excited using an adjustable diode laser (Coherent Inc., Santa Clara, CA, USA) with 300 mA current at the wavelength 980 nm. All optical measurements were carried out at room temperature.

3. Results

3.1. Density and chemical durability

Fig. 1 shows the density of PAZE glasses and PAZEY glasses. The density significantly increases as increasing concentrations of Er_2O_3 and Yb_2O_3. Fig. 2 shows the dissolution rate of PAZE glasses and PAZEY glasses in distilled water at 100 °C for 1 h. The dissolution rate decreases with increasing concentrations of Er_2O_3 and Yb_2O_3. For PAZE glasses, the dissolution rate decreases from 7.12×10^{-6} to 2.11×10^{-6} g/cm^2 h as the Er_2O_3 concentration increases from 1 to 10 mol%. Similar results are observed in PAZEY glasses.

Tables 1 and 2 list the glass transition temperature (T_g), glass softening temperature (T_s) and thermal expansion coefficient (α) for PAZE glasses and PAZEY glasses, respectively. Both tables indicate that the values of T_g and T_s increase as increasing concentrations of Er_2O_3 and Yb_2O_3, whereas the values of α decrease.

The ^{27}Al MAS-NMR spectrum of the basic PAZ glass is shown in Fig. 3. Three peaks near +32, +4 and −20 ppm are assigned to AlO_4, AlO_5 and AlO_6, respectively [25,26]. In accordance with Fig. 3, a larger

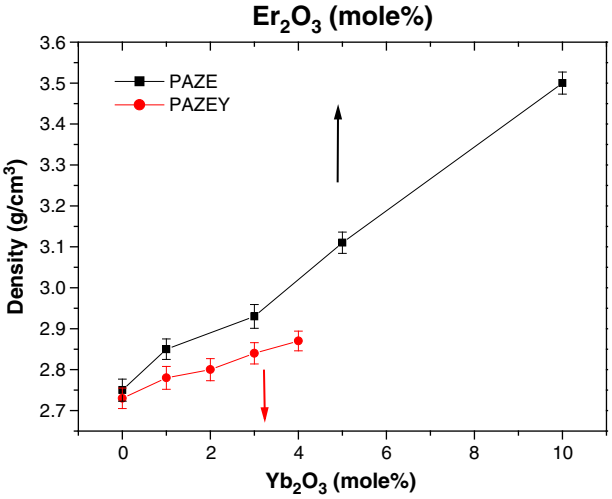

Fig. 1. Density of $60P_2O_5$–$10Al_2O_3$–(30−x) ZnO−x Er_2O_3 (PAZE) glasses and $60P_2O_5$–$10Al_2O_3$–(25−y) ZnO–$5Er_2O_3$–yYb_2O_3 (PAZEY) glasses.

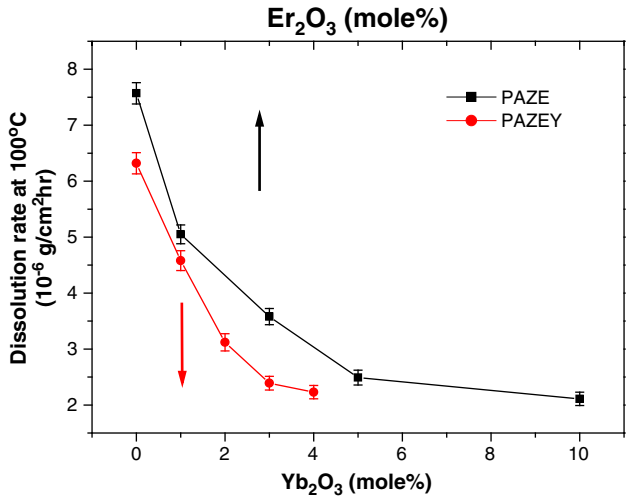

Fig. 2. Dissolution rate of $60P_2O_5$–$10Al_2O_3$–(30−x) ZnO−x Er_2O_3 (PAZE) glasses and $60P_2O_5$–$10Al_2O_3$–(25−y) ZnO–$5Er_2O_3$–yYb_2O_3 (PAZEY) glasses.

amount of bonded AlO_4 forms to alter and strengthen the glasses network, leading to a decrease in thermal expansion coefficient and increase in T_g, T_d and chemical durability.

Fig. 4 shows FTIR spectra of the PAZ glasses with different ZnO concentrations, 20 to 40 mol%, in the frequency range 400–1400 cm^{-1}. The spectra indicate the five absorption bands at 1270 cm^{-1}, 1160 cm^{-1}, 950 cm^{-1},770 cm^{-1} and 730 cm^{-1}, respectively. The absorption band near 1270 cm^{-1} is assigned to out-of-chain $(PO_2)_{as}$, the asymmetric stretching motion of the two non-bridging oxygen atoms bonded to phosphorus atoms (PO_2) in the Q^2 phosphate tetrahedron [27–29]. The absorption band near 1160 cm^{-1} is assigned to the PO_2 symmetric stretching motion, $(PO_2)_s$ [28]. The chain length of phosphate molecule chain decreases as ZnO concentration increases. Therefore, the intensity of $(PO_2)_{as}$ and $(PO_2)_s$ increases with increasing number of non-bridging oxygen atoms. The absorption band near 950 cm^{-1} is assigned to $(P–O–P)_{as}$, the asymmetric stretching motion of oxygen atoms bridging two phosphorus atoms in the Q^3 phosphate tetrahedron. The absorption band near 770 cm^{-1} and 730 cm^{-1} are assigned to the symmetric stretching motions of the in-chain P–O–P linkages, $(P–O–P)_s$ in the Q^2 and Q^1 phosphate tetrahedron, respectively [2,29]. According to Koo et al. [2], the absorption bands for $(P–O–P)_s$ shift to higher wavenumber due to lower bond angle of P–O–P linkages, shortening of phosphate chain length and smaller size of metal cations. When the concentration of ZnO is less than 50 mol%, the Zn^{2+} ions will play the role of glass-modifier. The (Zn…) $^-$O–P–O $^-$(Zn…) linkages will form due to the combination of Zn^{2+} ions and non-bridging oxygen atoms [28]. Moreover, the phosphate chain length decreases as the concentration of Zn^{2+} increases. Therefore the absorption bands for $(P–O–P)_s$ shift to higher wavenumber with increasing Zn^{2+} concentration.

Table 1
Thermal expansion coefficient(α), glass transformation temperature (T_g) and glass softening temperature (T_s) of $60P_2O_5$–$10Al_2O_3$–(30−x) ZnO–x Er_2O_3 (PAZE) glasses.

Er_2O_3 (mol%)	α (×10^{-7}/°C) (±2)	T_g (°C) (±2)	T_s (°C) (±2)
0	62	551	597
1	61	553	600
2	60	560	600
3	58	564	602
4	56	573	610
5	55	584	619
10	46	597	632

Table 2
Thermal expansion coefficient(α), glass transformation temperature (T_g) and glass softening temperature (T_s) of $60P_2O_5$–$10Al_2O_3$–(25−y)ZnO–$5Er_2O_3$–yYb_2O_3 glasses.

Yb_2O_3 (mol%)	α (×10^{-7}/°C) (±2)	T_g (°C) (±2)	T_s (°C) (±2)
0	62	555	600
1	59	556	608
2	54	559	611
3	48	561	615
4	45	563	621

Fig. 5 shows FTIR spectra of PAZE glasses with different Er_2O_3 concentrations in the frequency range 400–1400 cm^{-1}. The intensity of absorption band $(PO_2)_{as}$ increases as the concentration of Er_2O_3 increases. Fig. 5 also reveals that the absorption band $(P–O–P)_s$ shifts to lower wavenumber as concentration of Er_2O_3 increases. This is because the bond angle of P–O–P linkages increases when P–O^- …Zn^{2+} linkages are replaced by P–O^- …Er^{3+} linkages in the glass network. The result is similar to the study of Nelson et al. [30].

The absorption and fluorescence spectra of PAZE glasses versus different doping concentrations of Er_2O_3 were explored. Fig. 6 indicates the absorption spectra of PAZE glasses. The absorption spectra consist of two absorption bands at about 1492 and 1535 nm, respectively. The two bonds correspond to the absorption from the ground state $^4I_{15/2}$ to the excited states $^4I_{13/2}$ [31]. The absorbance increases with increasing Er_2O_3 concentration. When the Er_2O_3 concentration is 10 mol%, the strongest absorption band is observed.

Fig. 7 indicates the fluorescence spectra of the PAZE glasses, whose peaks locate at 1492 nm and 1535 nm, respectively. The intensity of emission peak and the values of full-width-at-half-maximum (FWHM) increase with Er_2O_3 concentration. However, the foregoing values decrease when the concentration of Er_2O_3 exceeded ~5 mol%.

Fig. 8 depicts the absorption spectra of PAZEY glasses with different amounts of Yb_2O_3 at the wavelength 978 nm. The figure depicts two absorption bands peaking at 920 nm and 978 nm, respectively. For these glasses, the strongest absorption band peak is observed at 978 nm. The absorbance of the glasses increases with increasing Yb^{3+} concentration. However, a reduction of absorbance is observed when Yb^{3+} concentration is greater than 3 mol%. Fig. 8 also indicates that the PAZEY glasses exhibit an absorption broader band between 870 and 1060 nm due to the ground state absorption band for $^2F_{5/2}$ excitation state of Yb^{3+} coinciding with the $^4I_{11/2}$ excitation state of Er^{3+}.

The emission spectra of PAZEY glasses are observed under continuous excitation pumped using 978 nm in Figs. 9 and 10. Fig. 9 depicts the emission spectra of PAZEY glasses at wavelength range from 850 to 1100 nm. The emission peaks at 978 nm and 1004 nm

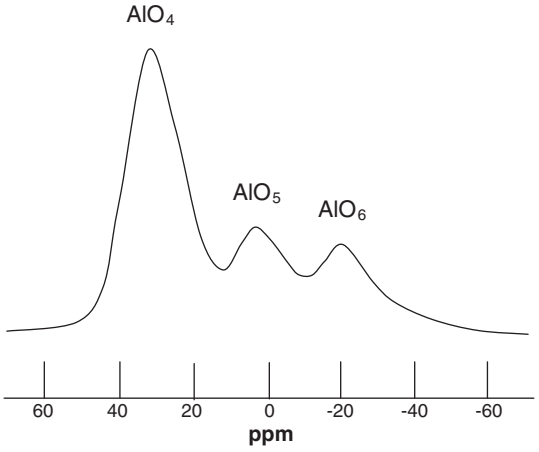

Fig. 3. ^{27}Al MAS-NMR spectrum of the $60P_2O_5$–$10Al_2O_3$–30ZnO (PAZ) glass.

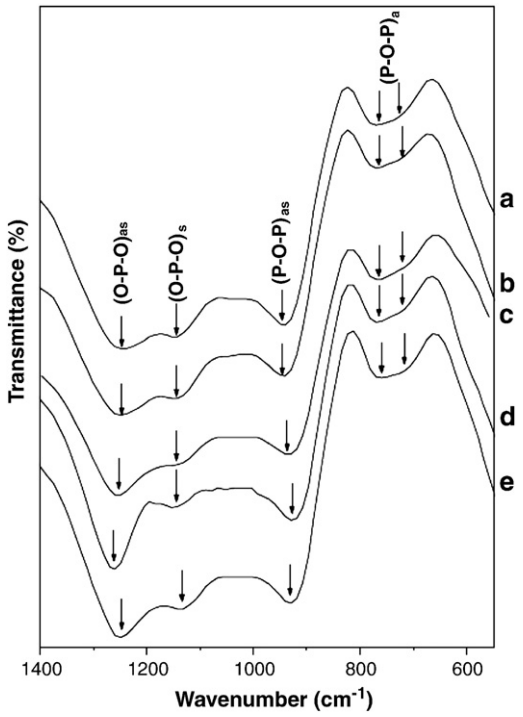

Fig. 4. FTIR spectra of $60P_2O_5$–x Al_2O_3–(40−x) ZnO (PAZ) glasses: (a) x = 20; (b) x = 25; (c) x = 30; (d) x = 35 and (e) x = 40.

correspond to the transition from the ground state $^2F_{7/2}$ to an excited state $^2F_{5/2}$. According to Fig. 9, the intensity of emission peak increases obviously as increasing Yb_2O_3 concentration. The strongest intensity of emission peak is observed when the concentration of Yb_2O_3 is about 4 mol%. Also, Fig. 9 indicates that the intensity of emission peak of Er^{3+}/Yb^{3+}-codoped glasses is much stronger than that of Er^{3+}-doped glasses. Fig. 10 depicts the fluorescence spectra of PAZEY glasses at wavelength range 1470 nm to 1590 nm. The main emission

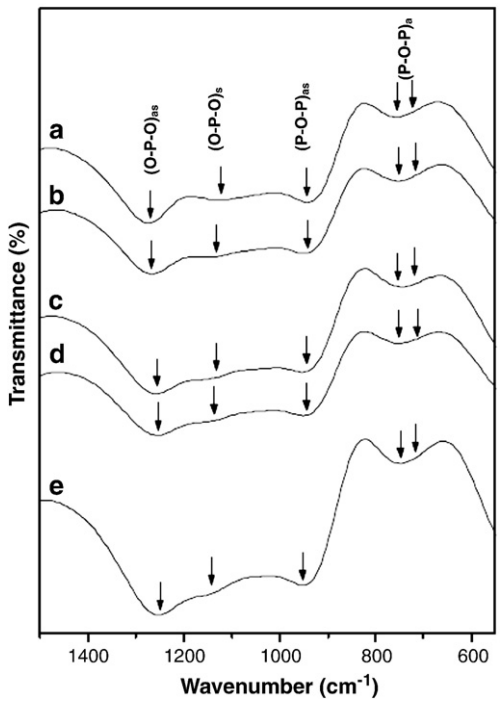

Fig. 5. FTIR spectra of $60P_2O_5$–$10Al_2O_3$–(30−x) ZnO–x Er_2O_3 (PAZE) glasses (a) x = 0; (b) x = 1; (c) x = 3; (d) x = 5 and (e) x = 10.

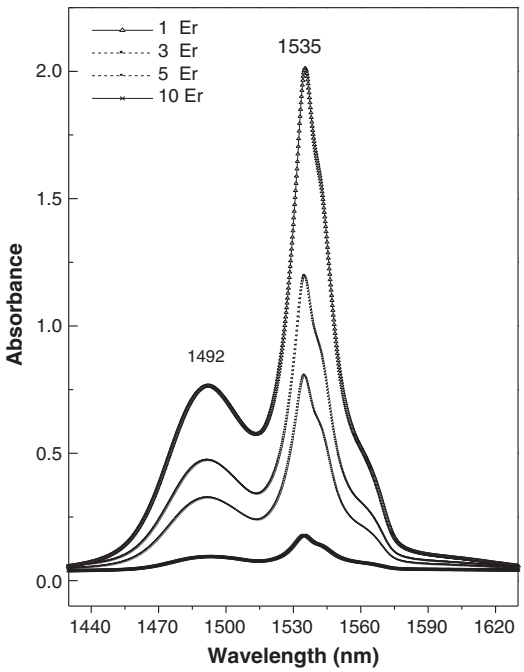

Fig. 6. Absorption spectra of $60P_2O_5$–$10Al_2O_3$–(30−x) ZnO−x Er_2O_3 (PAZE) glasses peaking at wavelength 1535 nm.

peak is at 1535 nm and its intensity increases with increasing Yb_2O_3 concentration. However, the intensity of emission peak is slightly decreased when the Yb_2O_3 concentration is higher than 3 mol%.

4. Discussion

4.1. Effect of Er_2O_3 and Yb_2O_3 on properties

In this study, the maximum concentration of Er_2O_3 and Yb_2O_3 are about at 10 mol% and 4 mol%, respectively. The density significantly increases as increasing concentrations of Er_2O_3 and Yb_2O_3 (Fig. 1). This is because the atomic weights of both Er and Yb are greater than

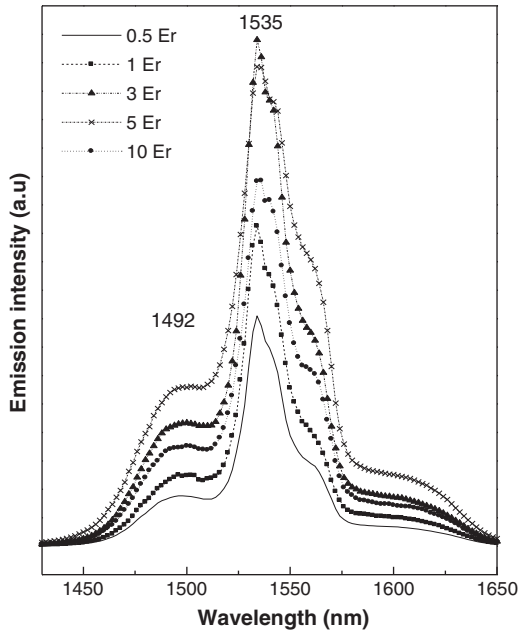

Fig. 7. Emission spectra of $60P_2O_5$–$10Al_2O_3$–(30−x) ZnO−x Er_2O_3 (PAZE) glasses peaking at wavelength 1535 nm.

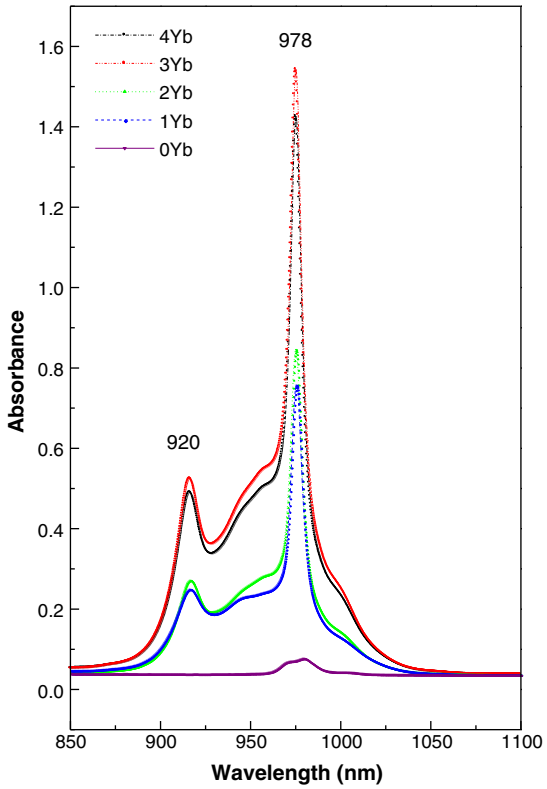

Fig. 8. Absorption spectra of $60P_2O_5$–$10Al_2O_3$–(25−y) ZnO–$5Er_2O_3$–yYb_2O_3 (PAZEY) glasses peaking at wavelength 978 nm.

those of the rest elements in the glass matrix [27]. The dissolution rate decreases with increasing concentrations of Er_2O_3 and Yb_2O_3 (as shown in Fig. 2). Bowron et al. disclosed that the chemical durability of phosphate glasses can be improved by the addition of various rare-earth ions [32]. In accordance with the literature [32], Er^{3+} and Yb^{3+} play the role as glass network-modifier in the phosphate glass when

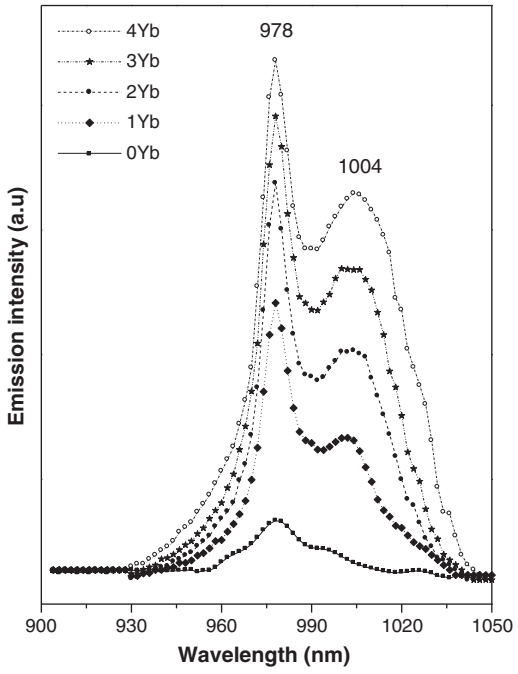

Fig. 9. Emission spectra of $60P_2O_5$–$10Al_2O_3$–(25−y) ZnO–$5Er_2O_3$–yYb_2O_3 (PAZEY) glasses peaking at wavelength 978 nm.

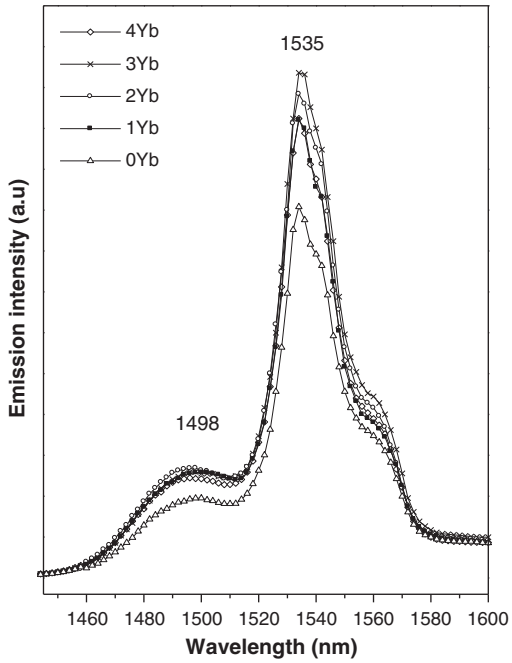

Fig. 10. Emission spectra of $60P_2O_5$–$10Al_2O_3$–(25−y) ZnO–$5Er_2O_3$–yYb_2O_3 (PAZEY) glasses peaking at wavelength 1535 nm.

the coordination number of Er^{3+} and Yb^{3+} is greater than six. The presence of Er^{3+} and Yb^{3+} provides strong ionic bonding between phosphate chains, results in the repression on the hydration as glass at the one hand, and inhibition of the diffusion of water molecules into the glass network on the other hand [33]. Therefore, in this study, the addition of Er_2O_3 and Yb_2O_3 can effectively reduce the dissolution rate of the studied glasses.

The values of T_g, T_s and α relate to the cross-linking density, bonding strength between phosphate chains, and the properties of modifiers of the glasses [34]. Both Tables 1 and 2 indicate that the values of T_g and T_s increase as increasing concentrations of Er_2O_3 and Yb_2O_3 because of the strong ionic bonding between Er^{3+} and/or Yb^{3+} and the O^{2-} anions in the glass network. These bonds strengthen the network by creating cross-linking between phosphate chains [27,33]. The values of α decrease with increasing concentrations of Er_2O_3 and Yb_2O_3 as is also attributed to the increment of cross-linking density and bonding strength in the glass network. In addition, Er^{3+} and Yb^{3+} locate in the glass network structure as the glass modifiers which provide strong ionic bonds with nearby anions in the glass network [27,33]. Aluminum coordination in a phosphate glass has a significant effect on thermal and chemical properties of the glass. In accordance with Fig. 3, a larger amount of bonded AlO_4 forms to alter and strengthen the glasses network, leading to a decrease in thermal expansion coefficient and increase in T_g, T_d and chemical durability.

4.2. Effect of Er_2O_3 and Yb_2O_3 on fluorescence properties

In Fig. 7, the intensity of emission peak and the values of full-width-at-half-maximum (FWHM) increase with Er_2O_3 concentration. However, the foregoing values decrease when the concentration of Er_2O_3 exceeded ~5 mol%. According to literature [22,35,36] the effects from cooperative upconversion and energy transfer become stronger as increasing rare-earth concentrations, because of the decrement of distance between any two ions. However, excess Er^{3+} ions will lead to formation of ion pairs and clusters, thus, the reduction of quantum efficiency of the $^4I_{13/2} \rightarrow {}^4I_{15/2}$ emission and high non-radiative losses occur.

As shown in Figs. 9 and 10, these spectra represent the energy transfer from Yb^{3+} to Er^{3+} (i.e., $^2F_{5/2} + {}^4I_{15/2} \rightarrow {}^2F_{7/2} + {}^4I_{11/2}$). In other

words, Yb^{3+} ions on the fundamental level $^2F_{7/2}$ absorbing the 980 nm pump light energy, are excited to the excited level $^2F_{5/2}$, then rapidly transfer their energy to neighboring Er^{3+} ions on the fundamental level $^4I_{15/2}$, and then Er^{3+} ions are excited to the excited level $^4I_{11/2}$. However, since the excited level $^4I_{11/2}$ is unstable, Er^{3+} ions rapidly decay to the meta-stable level $^4I_{13/2}$, yielding fluorescence at wavelength 1535 nm [37]. According to Fig. 9, the intensity of emission peak increases obviously as increasing Yb_2O_3 concentration. The strongest intensity of emission peak is observed when the concentration of Yb_2O_3 is about 4 mol%. Also, Fig. 9 indicates that the intensity of emission peak of Er^{3+}/Yb^{3+}-codoped glasses is much stronger than that of Er^{3+}-doped glasses.

Fig. 10 illustrates that the main emission peak is at 1535 nm and its intensity increases with increasing Yb_2O_3 concentration. This is attributed to the fact that Yb^{3+} plays a role of sensitizer in the Er^{3+}/Yb^{3+}-codoped PAZEY glasses because of its strong absorption at wavelength 980 nm and the excited level $^2F_{5/2}$ of Yb^{3+} ion is close to the excited level $^4I_{11/2}$ of Er^{3+} ion. Furthermore, the $^2F_{5/2}$ energy level of Yb^{3+} ion is higher than the energy of meta-stable level $^4I_{13/2}$ for the Er^{3+} ion. Therefore, the energy transfer processes for populating the meta-stable level $^4I_{13/2}$ is markedly enhanced. For these reasons, the intensity of emissions peak in the Er^{3+}/Yb^{3+}-codoped PAZEY glasses is stronger than that in the Er^{3+}-doped PAZE glasses. However, the intensity of emission peak is slightly decreased when the Yb_2O_3 concentration is higher than 3 mol%. This is attributed to the appearance of clustering and the concentration quenching effect at high rare-earth concentrations in most of glass systems [12,23,24].

The absorption cross-section, σ_a, of the transition of Er^{3+} ions from fundamental level $^4I_{15/2}$ to meta-stable level $^4I_{13/2}$ can be calculated from the absorption spectrum:

$$\sigma_a = \frac{1}{N \times \ell} \ln\left(\frac{I_0}{I}\right) \quad (1)$$

where I_0/I is absorbance, ℓ the thickness of glass specimen, and N is the concentration of Er^{3+} or Yb^{3+} ions doping in glass. The emission cross-section, σ_e, at 1535 nm can be calculated from McCumber theory [38,39]. The absorption and stimulated emission cross-section are related by:

$$\sigma_e = \sigma_a \exp\left[\frac{(\varepsilon - h\nu)}{KT}\right] \quad (2)$$

where σ_a and σ_e are the absorption and calculated emission cross-section, respectively, ν the photon frequency, ε is the net free energy required to excite one Er^{3+} ion from the $^4I_{15/2}$ to $^4I_{13/2}$ states at temperature T, h is the Planck constant and k is the Boltzmann constant. The calculation of absorption cross-section (σ_a), emission cross-section (σ_e) and values of FWHM of PAZE glasses and some other glass systems are listed in Table 3. Obviously, values of the emission cross-section, σ_e, of PAZE glasses are greater than those reported in the literature [40–43]. In addition, the FWHM values are also close to those reported in the literature [40–43]. In general, the values of FWHM and σ_e are very important parameters for the applications in optical amplifier [44,45] because the gain bandwidth of an amplifier can be evaluated by $\sigma_e \times$ FWHM. The bigger the value of $\sigma_e \times$ FWHM, the greater is optical amplification.

In this study, the maximum emission cross-section, σ_e, of 3 mol% Er-doped PAZE glass is 7.64×10^{-21} cm^2 at wavelength 1535 nm. From Table 3, we find that the maximum value of $\sigma_e \times$ FWHM is 327.8 when the concentration of $Er^{3+}$is 5 mol%. Comparing with various glass systems as shown in Table 3, optical properties of 5 mol% Er^{3+}-doped PAZE glass are obviously better than those of the Er^{3+}-doped silicate, other phosphate or even the germanate glasses.

Table 3
The calculation for absorption and emission cross-section of rare-earth doped glasses at wavelength 1535 nm: $60P_2O_5$–$10Al_2O_3$–(30−x) ZnO−x Er_2O_3 (PAZE) glasses and compare with other glasses.

Glasses	σ_a ($\times 10^{-21}$ cm^2)	σ_e ($\times 10^{-21}$ cm^2)	FWHM	FWHM$\times\sigma_e$
1 mol% Er	4.22	4.87	29	151.0
3 mol% Er	6.32	7.64	33	275.1
5 mol% Er	6.45	7.45	44	327.8
10 mol% Er	6.62	7.30	37	270.1
FP1E[12]	6.50	7.50	30	225.0
FP3E[12]	6.69	7.72	35	270.5
FP5E[12]	6.71	7.75	40	310.0
Germanate[35]		5.68	53	301.0
Phosphate[36]		6.40	37	236.8
Silicate[37]		5.50	45	247.5
[38]		5.50	40	220.0
Tellurite[38]		7.50	65	487.0

5. Conclusions

Structure, the thermal, chemical and optical properties of Er^{3+}-doped and Er^{3+}/Yb^{3+}-codoped P_2O_5–Al_2O_3–ZnO (PAZ) glasses were investigated. The glass transition temperature (T_g) and glass softening temperature (T_s) increase with increasing concentrations of Er_2O_3 and Yb_2O_3, whereas thermal expansion coefficient (α) and chemical durability decrease. FTIR results indicated five absorption bands at 1270 cm^{-1}, 1160 cm^{-1}, 950 cm^{-1}, 770 cm^{-1} and 730 cm^{-1}, respectively. The band shift and intensity of absorption bands relate to ZnO and Er_2O_3 concentrations in the PAZ glasses and PAZE glasses. The absorption and emission intensities of Er-doped PAZE and Er^{3+}/Yb^{3+}-codoped PAZEY glasses were studied. The absorption and emission intensities increase as concentrations of Er_2O_3 and Yb_2O_3 increase. However, the emission intensity significantly decreases when the concentration of Er_2O_3 is higher than 3 mol% for Er^{3+}-doped PAZE glasses, and that of Yb_2O_3 higher than 4 mol% for Er^{3+}/Yb^{3+}-codoped PAZEY glasses. The maximum emission cross-section, σ_e, of 3 mol% Er-doped PAZE glass is 7.64×10^{-21} cm^2 at wavelength 1535 nm. The maximum value of $\sigma_e \times$ FWHM is 327.8 when the concentration of Er^{3+} is about at 5 mol%. In addition, optical properties of 5 mol% Er^{3+}-doped PAZE glass are obviously better than those of the Er^{3+}-doped silicate, other phosphate or even germanate glasses.

References

[1] C.Z. Weng, J.H. Chen, P.Y. Shih, Mater. Chem. Phys. 115 (2009) 628.
[2] J. Koo, B.S. Bae, H.K. Na, J. Non-Cryst. Solids 212 (1997) 173.
[3] S. Rani, S. Sanghi, A. Agarwal, N. Ahlawat, J. Alloys Compd 477 (2009) 504.
[4] C.A. Click, R.K. Brow, T.M. Alam, J. Non-Cryst. Solids 311 (2002) 294.
[5] Sherief M. Abo-Naf, N.A. Ghoneim, H.A. Ei-Batal, J. Mater. Sci. 15 (2004) 273.
[6] R.K. Brow, D.R. Tallant, J. Non-Cryst. Solids 222 (1997) 396.
[7] P.A. Tick, Phys. Chem. Glasses 25 (1984) 149.
[8] B.C. Sales, L.A. Boatner, J. Non-Cryst. Solids 79 (1986) 83.
[9] J.H. Campbell, T.I. Suratwala, J. Non-Cryst. Solids 263–264 (2000) 318.
[10] S.T. Reis, M. Karabulut, D.E. Day, J. Non-Cryst. Solids 292 (2001) 150.
[11] H. Doweidar, Y.M. Moustafa, K. Ei- Egili, I. Abbas, Phys. Chem. Glasses 37 (2005) 91.
[12] S.W. Yung, H.J. Lin, Y.Y. Lin, R.K. Brow, Y.S. Lai, J.S. Horng, T. Zhang, Mater. Chem. Phys. 117 (2009) 29.
[13] K. Binnemans, R.V. Deun, C. Gorller-Walrand, J.L. Adam, J. Non-Cryst. Solids 238 (1998) 11.
[14] Z. Liu, C. Qi, S. Dai, Y. Jiang, L. Hu, Opt. Mater. 21 (2003) 789.
[15] R. Francini, F. Giovenale, U.M. Grassano, P. Loporta, S. Taccheo, Opt. Mater. 13 (2000) 417.
[16] A.J. Barbosa, F.A. Dias Filho, Y. Messaddeq, S.T.L. Ribeiro, P.R. Goncalves, S.R. Luthi, A.S.L. Gomes, J. Non-Cryst. Solids 352 (2006) 3636.
[17] L. Zhang, H. Hu, F. Lin, Mater. Lett. 47 (2001) 189.
[18] B. Majaron, M. Lukac, M. Copic, IEEE J. Quantum Electron. 31 (1995) 301.
[19] S. Taccheo, G. Sorbello, S. Longhi, P. Laporta, Opt. Quant. Electron. 31 (1999) 249.
[20] V.P. Gapontsev, S.M. Matitsin, A.A. Iseneev, V.B. Kravchenko, Opt. Laser Technol. 14 (1982) 189.
[21] X. Zou, H. Toratani, Phys. Rev. B 52 (1995) 15889.
[22] L. Zhang, H. Hu, C. Qi, F. Lin, Opt. Mater. 17 (2001) 371.
[23] S.Y. Chen, C.C. Ting, W.F. Hsieh, Thin Solid Films 434 (2003) 171.
[24] H. Desirena, E. Dela Rosa, L.A. Diaz-Torres and G.A. Kumar, 28 (2006) 560

[25] J.F. Ducel, J.J. Videau, M. Couzi, Phys. Chem. Glasses 34 (1993) 212.
[26] G. Gongyi, Mater. Res. Bull. 34 (1999) 621.
[27] P.Y. Shih, Mater. Chem. Phys. 84 (2004) 151.
[28] R.K. Brow, D.R. Tallant, S.T. Myers, C.C. Phifer, J. Non-Cryst. Solids 191 (1995) 45.
[29] K. Meyer, J. Non-Cryst. Solids 209 (1997) 227.
[30] B.N. Nelson, G.J. Exarhos, J. Non-Cryst. Solids 71 (1979) 2739.
[31] H. Chen, Y.H. Liu, Y.H. Zhou, Z.H. Jiang, J. Alloys. Compd. 397 (2005) 286.
[32] D.T. Browron, G.A. Saunders, R.J. Rainford, H.B. Senin, Phys. Rev. B 53 (1996) 5268.
[33] J.A. Sampaio, S. Gama, Phys. Rev. B 69 (2004) 104203.
[34] J.Y. Ding, S.W. Yung, P.Y. Shih, Phys. Chem. Glasses 43 (2002) 300.
[35] M. Karabulut, E. Metwalli, R.K. Brow, J. Non-Cryst. Solids 283 (2001) 211.
[36] M. Rico, M.C. Pujol, X. Mateos, J. Massons, C. Zaldo, M. Aguilo, F. Diaz, J. Alloys. Compd. 323–324 (2001) 362.
[37] Y.H. Wang, C.S. Ma, D.L. Li, D.M. Zhang, Opt. Laser Technol. 41 (2009) 545.
[38] D.E. McCumber, Phys. Rev. B 134 (1964) 299.
[39] D.E. McCumber, Phys. Rev. B 136 (1964) 954.
[40] H. Lin, E.Y.B. Pun, S.Q. Man, J. Opt. Soc. Am. B 18 (2006) 602.
[41] S. Jiang, T. Luo, B.C. Hwang, S. Fred, S. Karine, L. Jacques, P. Nasser, J. Non-Cryst. Solids 263–264 (2000) 364.
[42] J. Yang, S. Dai, L. Hu, Z. Jiang, S. Li, Acta Opt. Sin. 23 (2003) 210.
[43] X. Zou, T. Izumitani, J. Non-Cryst. Solids 162 (1993) 68.
[44] J. Yang, S. Dai, Y. Zhou, L. Wen, L. Hu, Z. Jiang, J. Appl. Phys. 93 (2003) 983.
[45] P. Babu, H.J. Seo, K.H. Jang, K.U. Kumar, C.K. Jayasankar, Chem. Phys. Lett. 4 (2007) 162.